Trade-offs in adaptation to glycolysis and gluconeogenesis result in a preferential flux direction in central metabolism

Severin Schink[1]*, Dimitris Christodoulou[1,2]*, Avik Mukherjee[1], Edward Athaide[1], Uwe Sauer[2] and Markus Basan[1, #]

* Equal contribution

[1] Systems Biology Department, Harvard Medical School, 200 Longwood Ave, 02115 MA, USA

[2] Institute of Molecular Systems Biology, ETH Zurich, Zurich 8093, Switzerland

[#] Correspondence: markus@hms.harvard.edu

Microbes exhibit an astounding phenotypic diversity, including large variations in growth rates and their ability to adapt to sudden changes in conditions. Understanding such fundamental traits based on molecular mechanisms has largely remained elusive due to the complexity of the underlying metabolic and regulatory network. Here, we study the two major opposing flux configurations of central carbon metabolism, glycolysis and gluconeogenesis using a coarse-grained kinetic model. Our model captures a remarkable self-organization of metabolism in response to nutrient availability: key regulatory metabolites respond to the directionality of flux and adjust activity and expression levels of metabolic enzymes to efficiently guide flux through the metabolic network. The model recapitulates experimentally observed temporal dynamics of metabolite concentrations, enzyme abundances and growth rates during metabolic shifts. In addition, it reveals a fundamental limitation of flux based sensing: after nutrient shifts, metabolite levels collapse and the cell becomes 'blind' to direction of flux. The cell can partially overcome this limitation at the cost of three trade-offs between lag times, growth rates and metabolic futile cycling that constrain the efficiency of self-organization after nutrient shifts. We show that these trade-offs impose a preferential flux direction and can explain the glycolysis preference observed for *Escherichia coli*, *Saccharomyces cerevisiae* and *Bacillus subtilis*, which only shift fast to glycolysis, but slow to gluconeogenisis Remarkably, as predicted from the model, we experimentally confirmed this preference could also be reversed in different species. Indeed, *P. aeruginosa* shows precisely the opposite phenotypic patterns, switching very quickly to gluconeogenesis, but showing multi-hour lag times that sharply increase with pre-shift growth rate in shifts to glycolysis.

These trade-offs between opposing flux directions can explain specialization of microorganisms for either glycolytic or gluconeogenic substrates and can help elucidate the complex phenotypic patterns exhibited by different microbial species.

Introduction

Fast growth and quick physiological adaptation to changing environments are key determinants of fitness in frequently changing environments that microorganisms encounter in the wild. One example of such a switch happens when microbes deplete their primary nutrient. *Escherichia coli* preferentially utilizes hexose sugars like glucose that are metabolized via glycolysis (Gerosa et al., 2015a). To maximize growth on sugars, *E. coli* excretes substantial 'overflow' production of acetate, even the presence of oxygen (Basan et al., 2015a, 2017). This naturally leads to bi-phasic growth, where initial utilization of glucose is followed by a switch to acetate. Similar growth transitions from preferred glycolytic substrates to alcohols and organic acids ubiquitously occur for microbes in natural environments (Buescher et al., 2012; Otterstedt et al., 2004; Zampar et al., 2013). Since these fermentation products are all gluconeogenic, they require a reversal of the flux direction in the glycolysis pathway. In a previous work (Basan et al., 2020), we showed that multi-hour lag phases occur in shifts from glycolytic to gluconeogenic conditions and we observed a trade-off between growth rate and lag time, where faster growth before the shift resulted in long lager phases. We showed that these lag phases result from an inability of *E. coli* to establish net gluconeogenic flux, caused by the depletion of metabolite pools throughout the gluconeogenesis pathway, and similar obervations where made for *Bacillus subtilis* and the yeast *Saccharomyces cerevisiae*. For organisms with preference for glycolytic substrates, we showed that shifts in the opposite direction, from gluconeogenic substrates to glycolytic ones, occur much more quickly, in some cases without detectable lag phases (Basan et al., 2020).

These findings raise several fundamental questions: Why do shifts from glycolytic to gluconeogenic conditions result in lag times of many hours, while shifts from gluconeogenic to glycolytic conditions only take minutes? Is this preference for glycolysis a fundamental property of central metabolism, or rather an evolutionary choice? And why are microorganisms like *E. coli* or *S. cerevisiae* unable to overcome lag phases by appropriate allosteric and transcriptional regulation? At the core of these questions, is a gap in understanding of how central carbon metabolism adjusts itself to nutritional changes. Because most organisms can use both glycolytic and gluconeogenic substrates as sole carbon sources, central metabolism must self-organize to generate all required precursors for new biomass from both directions.

Over the last two decades metabolic models have made substaintial progress in describing metabolism during steady state exponential growth, elucidating the flux and regulatory network that govern the coordination of mirobial metabolism (Bennett et al., 2009; Bordbar et al., 2014; Chubukov et al., 2014; Gerosa et al., 2015b; Link et al., 2013; Noor et al., 2010, 2014; Vasilakou et al., 2016). Such metabolic model were successfully expanded to dynamics environments (Zampar et al., 2013; Chassagnole et al., 2002; Chakrabarti et al., 2013; Saa and Nielsen, 2015; Andreozzi et al., 2016; Yang et al., 2019), and used to gather vital information about metabolism, using perturbations (Link et al., 2013), stimulus response experiments (Chassagnole et al., 2002) or sequential nutrient depletion (Yang et al., 2019) to validate and improve metabolic models. But, dynamic changes of metabolism continue pose a considerable challenge, in particular when the proteome undergoes reorganization, as changes in enzyme abundances influence fluxes and metabolite concentrations, and vice-versa, metabolites regulate enzyme expression. The resulting explosion of parameters prevents accurately predicting how metabolism re-organizes, and how long this adaptation takes.

Here, we introduce a minimal kinetic model of central carbon metabolism to overcome this challenge. Our model focuses on the dynamics of key regulatory metabolites in central metabolism and couples metabolism to enzyme abundance, and enzyme expression to the concentration of regulatory metabolites, via allosteric and transcriptional regulation, flux dependent protein synthesis and growth. This self-consistent formulation of metabolism and growth bridges fast metabolic time scales with slow protein synthesis. As we demonstrate, our model can explain a major reorganization of metabolism in response to nurtients shifts: the switching on the directionality of metabolic flux between glycolysis and gluconeogenesis. Dependent on the required directionality of flux in central metabolism, enzymes catalyzing the required flux direction are expressed and catalytically active, while enzymes catalyzing the opposite flux are expressed at low levels and their activities are repressed by allosteric regulation. This self-organization is key for enabling fast growth and preventing costly futile cycling between metabolic reactions in opposing directions, which can inhibit flux and deplete ATP in the process. Crucially, the model reveals a choice of one preferred flux direction determined by the relative strength of different allosteric regulations and imposes that lag phases are constrained by tradeoffs with the amount of futile cycling and growth rate before the switch.

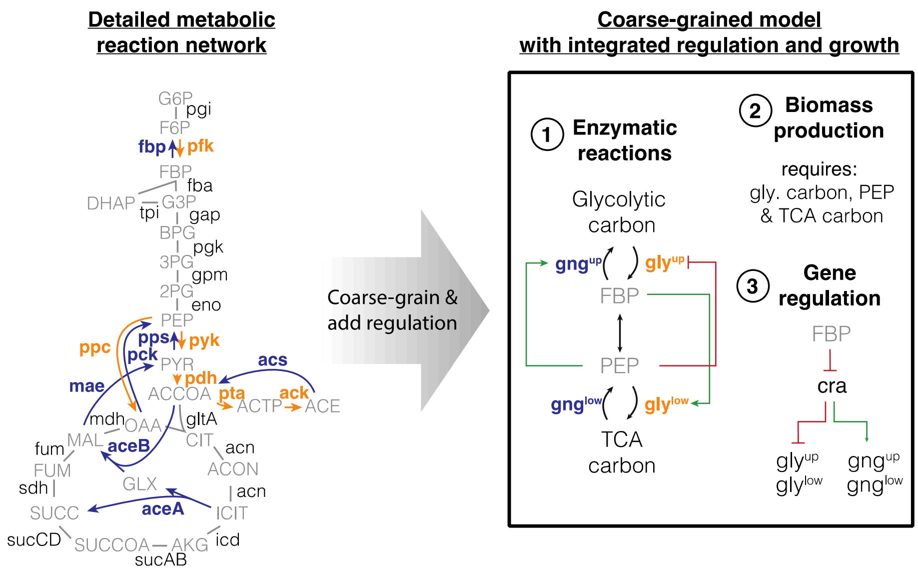

Mathematical formulation

1 Enzymatic reactions

Enzyme kinetics (modified Michaelis-Menten)

$$r_i = \phi_i k_{\mathrm{cat},i} \frac{c_i}{c_i + K_{\mathrm{M},i}} \left(c_i/c_i^*\right)^{\alpha_i} \qquad \text{Eq. (1)}$$

Kinetics of reversible 'super eno' reaction

$$r_{\mathrm{eno}+} = k_{\mathrm{eno}}^{+}\, \phi_{\mathrm{eno}}\, c_{\mathrm{FBP}}$$

$$r_{\mathrm{eno}-} = k_{\mathrm{eno}}^{-}\, \phi_{\mathrm{eno}}\, c_{\mathrm{PEP}}^{2} \qquad \text{Eqs. (2, 3)}$$

2 Biomass production

$$r_{\mathrm{BM}} = k_{\mathrm{cat,BM}} \frac{c_{\mathrm{GLY}}}{c_{\mathrm{GLY}}^*} \frac{c_{\mathrm{PEP}}}{c_{\mathrm{PEP}}^*} \frac{c_{\mathrm{TCA}}}{c_{\mathrm{TCA}}^*} \qquad \text{Eq. (4)}$$

3 Gene regulation

for gluconeogenic enzymes

$$\frac{\mathrm{d}\phi_j}{\mathrm{d}t} = \mu\left(\phi_j^*\left((1+x_j) - x_j \frac{c_{\mathrm{FBP}}(t)}{c_{\mathrm{FBP}}^*}\right) - \phi_i(t)\right) \qquad \text{Eq. (5)}$$

for glycolytic enzymes

$$\frac{\mathrm{d}\phi_i}{\mathrm{d}t} = \mu\left(\phi_i^*\left(x_i - (1-x_i) \frac{c_{\mathrm{FBP}}(t)}{c_{\mathrm{FBP}}^*}\right) - \phi_i(t)\right) \qquad \text{Eq. (6)}$$

Box 1 Integrated kinetic model of central carbon metabolism. The detailed metabolic reaction network of central carbon metabolism is coarse-grained to a minimal network, by combining irreversible glycolytic (orange) and gluconeogenic reactions (blue), as well as metabolites. Influx can either occur from glycolytic carbon sources (e.g. glucose) or TCA carbon sources (e.g. acetate). (1) Gatekeepers to the central section of glycolysis and gluconeogenesis are the two irreversible reactions (gly^{up}, gng^{up} and gly^{low}, gng^{low}) that feed and drain FBP and PEP. The irreversible reactions are allosterically regulated by FBP (Fructose 1-6-bisphosphate) and PEP (phosphoenolpyruvate), where 'outward' facing reactions are activated (green arrows) and 'inward' facing reactions are repressed (red arrow). Fluxes r_i of enzymes i depend on enzyme abundances ϕ_i, catalytic rates $k_{cat,i}$ and allosteric regulations, modeled as a Hill function below its maximal saturation $(c_j/c_j^*)^{\alpha_i}$, where c_j is the concentration of the regulatory metabolite and c_j^* is a reference concentration. Reversible fluxes are modeled with simple mass action kinetics. (2) Biomass production requires precursors from glycolytic carbons, PEP and TCA carbons, and is implemented in the model as single reaction that drains all three metabolites simultaneously at catalytic rate $k_{cat,BM}$. (3) Glycolytic and gluconeogenic enzymes are regulated by Cra, which is in turn modulated by FBP. In the model, we assume enzyme expression to linearly depend on FBP concentration c_{FBP} . Growth rate: μ, steady state abundance: ϕ_i^* , steady state concentration c_{FBP}^* and x_i & x_j modulate the sensitivity of regulation to FBP. Glycolytic and gluconeogenic enzymes are produced as part of protein synthesis. Thus in the model, flux through metabolism automatically leads to synthesis of metabolic enzymes and biomass production, resulting in dilution of existing enzymes.

Results

An integrated, self-consistent kinetic model of glycolysis / gluconeogenesis

Using a theoretical model we wanted to understand how microbes self-organize during glycolytic and gluconeogenic growth, and how the re-arrangement of this self-organization determines lag phases. The complexity of central metabolism with intertwined regulation at different levels in even comparably simply bacteria poses a challenge to quantitative mechanistic understanding because causal effects behind phenotypes are hard to trace to their molecular origins. We thus sought to construct a minimal model that focuses on the biochemical pathway topology in *E. coli*, and the key regulations that differentiate glycolysis and gluconeogenesis. The model, illustrated in Box 1, is based on topology of the biochemical network and allosteric and transcriptional regulation of glycolysis/gluconeogenesis that has been characterized for *E. coli* (Berger and Evans, 1991; Ramseier et al., 1995; Johnson and Reinhart, 1997; Pham and Reinhart, 2001; Kelley-Loughnane et al., 2002; Hines et al., 2006; Fenton and Reinhart, 2009). The defining features of the model are a set of irreversible reactions (one-directional black arrows in 'orange' and 'blue', Box 1) in the upper and lower part of central metabolism. While not irreversible in an absolute sense, so-called irreversible reactions are thermodynamically favored so much in one direction that they can be effectively considered as irreversible (Noor et al., 2014). As a result, these irreversible reactions in the glycolysis/gluconeogenesis pathway are catalyzed by distinct enzymes, depending on the directionality of flux in the glycolytic or the gluconeogenic direction ('bold font, blue/orange'). Expression levels of these key enzymes, combined with allosteric regulation and substrate levels, determine the flux through central metabolism.

There are two sets of irreversible reactions in *E. coli* central metabolism. First, the irreversible reaction between fructose-6-phosphate (F6P) and fructose 1,6-bisphosphate (FBP), catalyzed in the forward direction by 6-phosphofructokinase (PfkA) and backward by fructose-1,6-bisphosphatase (Fbp), which we refer to as *upper glycolysis/gluconeogenesis*, respectively. Second, two sets of enzymes that produce phosphoenolpyruvate (PEP) and pyruvate (PYR), respectively, which we coarse-grain into two effective enzymes, called *lower glycolysis/gluconeogenesis* (Box 1, left). While we do not explicitly consider the pentose phosphate pathway in our model, it can effectively be considered as an irreversible reaction of upper glycolysis (Stincone et al., 2015).

In *E. coli*, the activity of enzymes at these irreversible reactions is controlled by several known allosteric interactions: FBP allosterically activates lower glycolysis PykF (Valentini et al., 2000)**,** whereas PEP allosterically inhibits PfkA (Pham and Reinhart, 2001) and activates Fbp in upper glycolysis (Hines et al., 2006). Due to their central role we model the dynamics of FBP and PEP explicitly using modified Michaelis-Menten kinetics (Box 1, Eq. (1)). The flux that links FBP and PEP is the result of a series of reversible enzymatic reactions (see Box 1, left), which we coarse-grain into a single reversible reaction ('super-eno', bidirectional black arrow in Box 1, right) and model with mass action kinetics (Box 1, Eqs. (2, 3)).

To accurately model growth transitions, biomass production must be taken into account. Biomass production is connected to our model in three ways. First, biomass production requires metabolites and thus drains them from the metabolic network, which in our case concerns three coarse-grained glycolytic intermediates with a specific stochiometric ratio that is set by the biomass composition (Supporting Information, Sec. 3.7). This biomass production yields a drain of the three metabolites, modeled by linear dynamics (Box 1, Eq. (4)). Second, part of the newly synthesized biomass are the enzymes themselves, which are primarily regulated by the transcription factor Cra in *E. coli* (Cortay et al., 1994; Ramseier et al., 1995), which is itself repressed by binding of the metabolite Fructose-1-phosphate, closely related to fructose 1-6-bisphosphate (FBP) (Folly et al., 2018). As a first-order approximation, we assume that the expression level of glycolytic and gluconeogenic enzymes linearly depends on FBP (Kochanowski et al., 2013a) (Box 1, Eqs. (5-6)), which will be sufficient to reproduce the empirical enzyme abundances, as we will see later in the text. Third, biomass accumulation is equivalent to growth and results in dilution of existing enzymes proportional to growth rate (Box 1, Eqs. (5-6)).

In total, the model encompasses four irreversible reactions, each regulated allosterically by either FBP or PEP, and transcriptionally by FBP via cra, and one reversible reaction that connects FBP and PEP. We used measured metabolite concentrations for growth on glucose (Kochanowski et al., 2013a) and Michaelis constants (Berman and Cohn, 1970; Zheng and Kemp, 1995; Donahue et al., 2000) to constrain enzymatic parameters, and biomass yield (Link et al., 2008) and density (Basan et al., 2015b) on glucose to constrain fluxes. We used the level of futile cycling in the upper and lower reactions in exponential glucose growth conditions as fitting parameters such that the model reproduces the observed lag times in this paper, see SI Sec. 3.2 for details.

Central carbon metabolism self-organizes in response to substrate availability

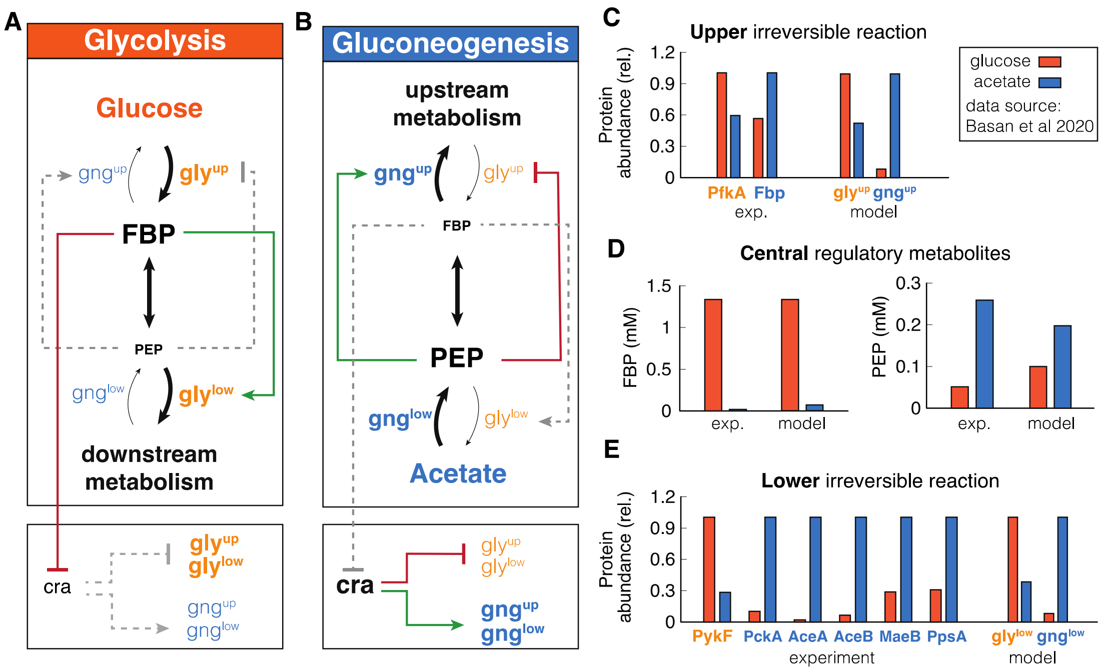

*Figure 1 Self-organization of metabolism in glycolysis and gluconeogenesis (**A** & **B**) Graphic summary of the reorganization in glycolysis and gluconeogenesis. Linewidth of reactions arrows indicate magnitude of flux. Font size of metabolites and enzymes indicate metabolite concentrations and enzyme abundances, respectively. Active regulation is indicated by red/green color, inactive regulation is grey and dashed. (**C**, **D** & **E**) Comparison of theoretical and experimental (from [3]) metabolite concentrations and enzyme abundances. Note the striking, differential regulation of FBP and PEP, high in one condition and low in the other.*

To test whether this simple model could recapitulate steady-state glycolytic and gluconeogenic growth conditions for *Escherichia coli*, we compared it to published metabolite and proteomics data for steady state exponential growth on glucose and acetate as sole carbon substrates (Basan et al., 2020). Indeed, the model reached distinct steady-states for glycolytic (Fig. 1A) and gluconeogenic conditions (Fig. 1B), consistent with experimental measurements Fig. 1C-E. The simulation elucidates how central metabolism self-organizes in response to glycolytic and gluconeogenic conditions and how allosteric and transcriptional regulation helps to optimize fluxes and minimize futile cycling. As shown in Fig. 1C, in 'orange', during glycolytic conditions, the simulation reached a steady-state with high FBP levels and low PEP levels, consistent with experimental metabolite measurements for FBP and PEP during growth on glucose. As illustrated in Fig. 1A, high FBP pool activates lower glycolysis, while the low PEP pool derepresses upper glycolysis and deactivates upper gluconeogenesis. This suppression of gluconeogenic fluxes in glycolysis reduces futile cycling, i.e., circular fluxes at the irreversible reactions, thereby streamlining metabolism.

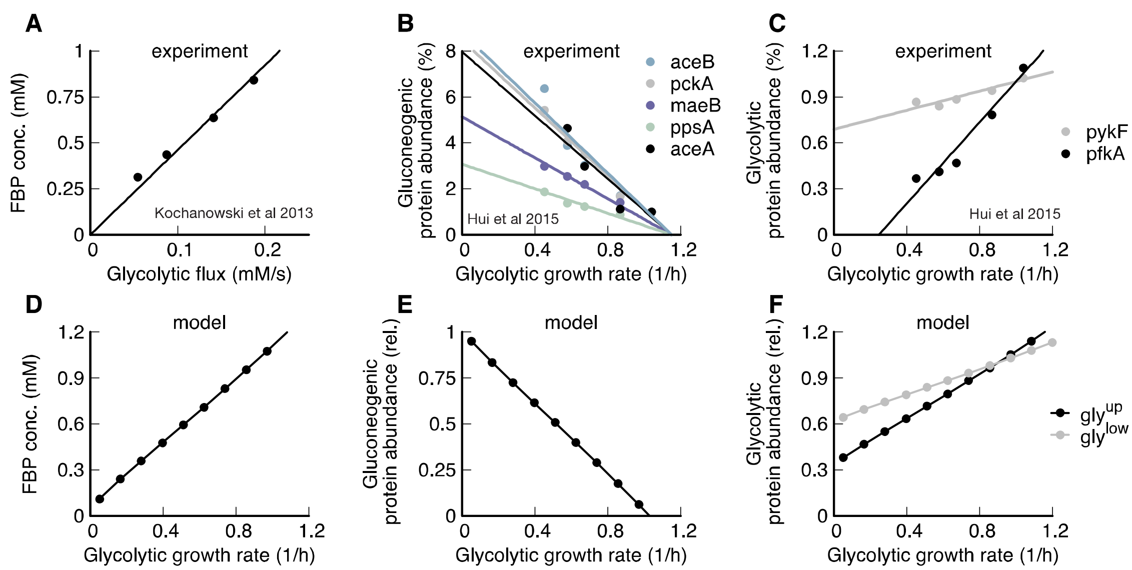

Figure 2 Metabolic state depends on growth rate. ***A*** *During glycolytic growth, FBP linearly increases with growth rate. Data: Ref. (Kochanowski et al., 2013b).* ***B*** *Gluconeogenic enzymes decrease linearly with glycolytic growth rate. Data: (Hui et al., 2015).* ***C*** *Glycolytic enzymes increase linearly with glycolytic growth rate. Data: Ref. (Hui et al., 2015).* ***D-F*** *Simulation results recapitulate experimental evidence.*

On a transcriptional level, the high FBP pool represses Cra, which in turn derepresses the expression of glycolytic enzymes and inhibits the expression of gluconeogenic enzymes. This results in high levels of glycolytic enzymes and low levels of gluconeogenic enzymes in the simulation (Fig. 1D & E, right panels), consistent with experimental findings from proteomics measurements (Fig. 1D & E, left panels).

In gluconeogenic conditions ('blue' in Fig. 1), we find precisely the complementary configuration of central carbon metabolism. Simulation and experiments show low FBP and high PEP pools (Fig. 1C). As illustrated in Fig. 1B, high PEP represses upper glycolysis and activates upper gluconeogenesis, while low FBP deactivates lower glycolysis. Low FBP also derepresses Cra, which leads to high expression of gluconeogenic enzymes and low expression of glycolytic enzymes (Fig. 1D, right panels), consistent with proteomics measurements (Fig. 1D & E, left panels).

Next we tested if the model could recapitulate how varying growth rates on glycolytic and gluconeogenic nutrients affects metabolite levels and protein expression (Gerosa et al., 2015a; Hui et al., 2015). In particular, it has been shown experimentally that FBP acts like a flux sensor and FBP concentration linearly increases with glycolytic flux (Fig. 2A, upper panel) (Kochanowski et al., 2013b), which is captured by our simulation (Fig. 2B), under the condition that the speed of the reversible reaction is slow compared to irreversible reactions. In this limit, PEP will be drained fast enough for the backward flux, Eq. (6), to be small, so that the net flux is dominated by the forward flux, Eq. (5), which is proportional to FBP. The linear increase of FBP concentration with growth rate results in a linear growth rate dependence of gluconeogenic and glycolytic enzyme abundances in the simulation, in good agreement with experimental measurements of enzyme abundances from proteomics (Fig. 2 compare B&C with E&F) (Hui et al., 2015). Together, these results show how central metabolism self-organizes dependent on the nutrient source, and that transcriptional and allosteric regulation of FBP and PEP alone suffice to achieve this major re-configuration.

Central carbon metabolism is primed for switches to glycolysis

Equipped with this model, we next address the question of understanding the mechanistic basis for the extended lag phases of *E. coli* upon nutrient shifts from glycolytic to gluconeogenic conditions (Basan et al., 2020; Kotte et al., 2014). After a shift from glucose to acetate, *E. coli* shows a long lag time with almost absent growth for around 5 h (Fig. 3A) (Basan et al., 2020), which can be captured by our model (Fig. 3B), if we fit pre-shift

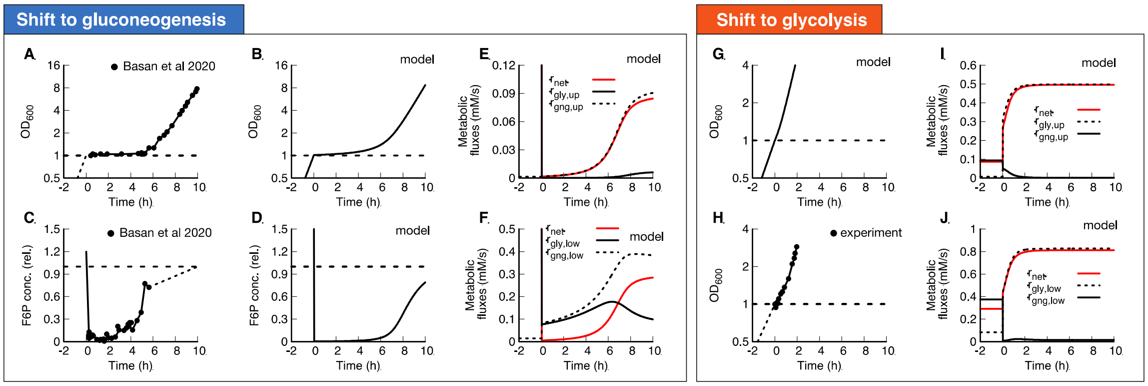

*Figure 3 Shifts between glycolysis and gluconeogenesis. (A) Experimental and (B) model of optical density after shift of E. coli from glucose to acetate. Growth shows a substantial lag before it recovers. (C) Experimental and (D) model of F6P (normalized to the final state) collapses after shit to acetate, and continues to stay low throughout lag phase. Because F6P is an essential precursor for biomass production, this limitation effectively stops biomass growth. (E&F) Fluxes of all irreversible reactions. Especially fluxes in lower glycolysis/gluconeogenesis are of equal magnitude, leading to a futile cycle, where no net flux (red line) through central carbon metabolism can be established. (**G-J**) Optical density and metabolic fluxes for the reversed shift from acetate to glucose shows immediate growth and no intermittent futile cycling. The dynamics of all enzyme abundances, regulation and fluxes for both shifts are shown in Fig. S1-5 in detail. The model also correctly predicts that enzyme abundances only adapt late in the lag phase (Fig. S6).*

futile cycling accordingly, see SI Sec. 3.2 for details. All model solutions shown in this paper are generated with the parameters generated from this fit. The model captures the slow adaptation of glycolytic and gluconeogenic enzymes, which only towards the end of the lag phase significantly change towards their new steady state values (Fig. S6). Investigating the origin of the growth arrest in the simulation, we found that during lag phase, the concentrations of upper glycolytic precursors (which includes F6P, G6P and above) remained very low compared to their steady-state values, which matches published experimental evidence of F6P measurements (Basan et al., 2020) (Fig. simulation: 3C, data 3D), indicating that the gluconeogenic flux limits formation of essential precursors for biomass formation. Thereby, according to Eq. (4) the depletion of this precursor limits growth rate during lag phase.

In the simulation, the F6P limitation is caused by low net fluxes in upper and lower gluconeogenesis (Fig. 3E &F, red lines). Previously, it was suggested that futile cycling between gluconeogenic and glycolytic enzymes could contribute to this flux limitation (Basan et al., 2020), supported by the observation that overexpression of glycolytic enzymes in upper or lower glycolysis strongly impaired switching and resulted in much longer lag times (Basan et al., 2020). The simulation allows us to probe the effect of futile cycling *in silico*, which cannot be directly measured experimentally. Indeed, we found for our default *E. coli* parameters that residual lower glycolytic flux almost completely canceled the flux from gluconeogenesis, i.e., $r_{\mathrm{gly}}^{\mathrm{low}} \approx r_{\mathrm{gng}}^{\mathrm{low}}$ (solid and dashed black lines in Fig. 3F), such that net flux remained close to zero (red line, Fig. 3E & F). Thus, this futile cycling appears to be the main reason for limiting net flux throughout the lag phase.

The biochemical network and regulation are almost completely symmetric with respect to the direction of flux, so one might naively expect a shift from gluconeogenesis to glycolysis to also result in a long lag. However, experimentally the shift in the opposite direction from gluconeogenesis to glycolysis occurs very quickly in *E. coli* (Fig. 3G) (Basan et al., 2020). Indeed, in simulations with our standard *E. coli* parameters, we found that central metabolism adjusted very quickly and growth resumed without a substantial lag phase (Fig. 3H). In striking contrast to the shift to gluconeogenesis, futile cycling played no role in the shift to glycolysis, because both upper and lower glycolytic fluxes got repressed immediately after the shift (Fig. 3I-J, solid black line), such that net flux can build up (Fig. 3I-J, red line). The absence of transient futile cycling, despite the symmetry of regulation and metabolic reactions, suggests that in *E. coli* allosteric and transcriptional regulations are 'primed' in the glycolytic direction.

Molecular cause of preferential directionality

To understand the molecular cause of the asymmetric response and lag phases, we investigated the role of allosteric and transcriptional regulation in our simulation. During steady state growth, the differential regulation during glycolysis and gluconeogenesis is achieved by PEP and FBP, the metabolites that are "sandwiched" between the two irreversible reactions and connected by a series of reversible enzymes, coarse-grained in our model into the 'super-enolase enzyme'. First, we focused on regulation during exponential growth and wanted to investigate how the cell achieves differential regulation of glycolytic and gluconeogenic enzymes using the metabolites FBP and PEP. In equilibrium, forward and backward reactions would balance, i.e., $r_{\mathrm{ENO}+} = r_{\mathrm{ENO}-}$, and no

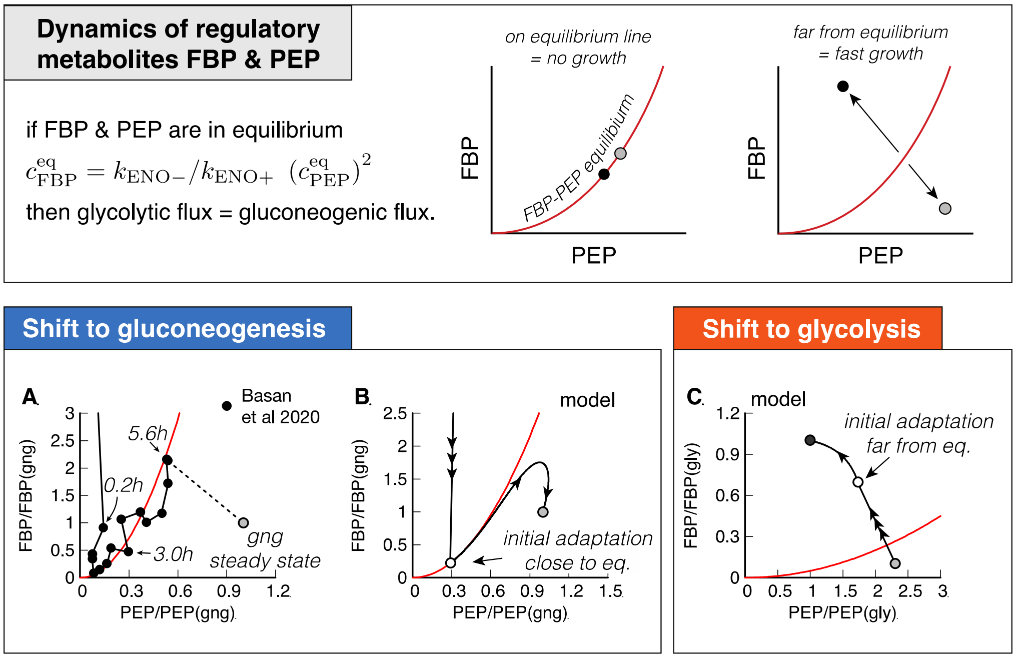

*Figure 4 Molecular cause for asymmetric recovery dynamics. (top) Graphical summary of dynamics of the regulatory metabolites FBP and PEP. Distance from the quadratic equilibrium line determines net metabolic flux and thus growth rate. (**A**) Recovery of FBP and PEP of after a shift from glucose to acetate, shows a distinctive joint increase, followed by an overshoot of FBP. Data from Ref. [4]. Red line is a quadratic guide to the eye. Final acetate steady state is drawn as grey symbol.(**B**) Model solution of FBP and PEP. After the fast collapse of metabolite levels (triple arrow to white circle), the dynamics closely follows the quadratic FBP-PEP equilibrium Eq. (**Error! Reference source not found.**. Eventually recovery will diverge away from the equilibrium line, towards the non-equilibrium steady states of gluconeogenesis (grey circle) (**C**) For a shift to glycolysis, metabolite levels do not collapse, but instead land already far from equilibrium (triple arrow to white circle), such that flux is immediately established, and recovery is quick.*

net flux can run through central metabolism, meaning that the cell cannot grow. Using Eqs. (2 & 3), the balance of forward and backward fluxes results in a fixed quadratic dependence of FBP and PEP in equilibrium,

$$c_{\mathrm{FBP}}^{\mathrm{eq}} = k_{\mathrm{ENO-}}/k_{\mathrm{ENO+}}\ \left(c_{\mathrm{PEP}}^{\mathrm{eq}}\right)^2. \quad (7)$$

In Figure 4 (top), we show a visual representation of the FBP-PEP relation. Close to the equilibrium, FBP and PEP levels go up and down together, rather than the opposing directions, as observed for glycolytic and gluconeogenic growth (Fig. 1A&B). This results in low net-flux and creeping growth. Hence, in steady state growth conditions, the equilibrium must be broken and FBP $\gg$ PEP or FBP $\ll$ PEP, such that either glycolytic flux is bigger than gluconeogenic, or vice-versa ($r_{\mathrm{ENO}+} \gg r_{\mathrm{ENO}-}$ and $r_{\mathrm{ENO}+} \ll r_{\mathrm{ENO}-}$, respectively). This is achieved by the irreversible reactions, which drain and supply metabolites to the 'super-enolase'. Because of the positive feedback between enzyme activity and non-equilibrium of the 'super-enolase', this regulation topology achieves differential regulation during glycolysis and gluconeogenesis. As we observed in the analysis of the glycolytic and gluconeogenic steady-states (Fig. 1), this differential regulation adjusts enzyme levels via transcriptional regulation and suppresses futile cycling at the irreversible reactions.

While regulation of central metabolism efficiently organizes FBP-PEP in a far from equilibrium state during exponential growth, nutrient shifts expose the limitations of this regulatory system. Metabolite measurements in the shift of *E. coli* from glucose to acetate show that levels of FBP and PEP drop within minutes of the shift to acetate, followed by a very slow joint increase of FBP and PEP over the course of hours, constituting the majority of the lag phase (Fig. 4A). This joint increase, rather than a differential increase, is the hallmark of a close-to-equilibrium state.

The slow recovery can be understood from the simulation, which shows that FBP and PEP proceed close to the equilibrium line of Eq. (7), where growth is slow (Fig. 4B). Strikingly, as shown in Fig. 3F, throughout most of the lag phase, higher gluconeogenic flux from increasing levels of gluconeogenic enzymes is almost completely lost to a corresponding increase in futile cycling, because increasing FBP activates lower glycolysis (instead of deactivating it) and thereby increases futile cycling. The overshoot of FBP in Fig. 4A (data) and Fig. 4B (model) corresponds to the breaking of the equilibrium, that finally allows the cell to establish net flux: PEP concentration is high enough to activate upper gluconeogenesis sufficiently to drain FBP via upper gluconeogenesis (see Fig. 3E). Lower FBP then shuts down futile cycling in lower glycolysis/gluconeogenesis (Fig. 3F), pushing FBP and PEP concentrations to a state far from the equilibrium line (see Fig. 4B) and allowing the cell to grow at a faster rate.

The fundamental difference between shifts to gluconeogenesis and glycolysis is that glycolytic shifts immediately land far from equilibrium (Fig. 4C, triple arrow to white circle), such that cells immediately grow at faster rates, allowing them to express the new enzymes needed to recover quickly. Thus, to understand why glycolytic shifts recover faster than gluconeogenic shifts, we need to understand why glycolytic shifts immediately land far from equilibrium, while gluconeogenic shifts land close to equilibrium.

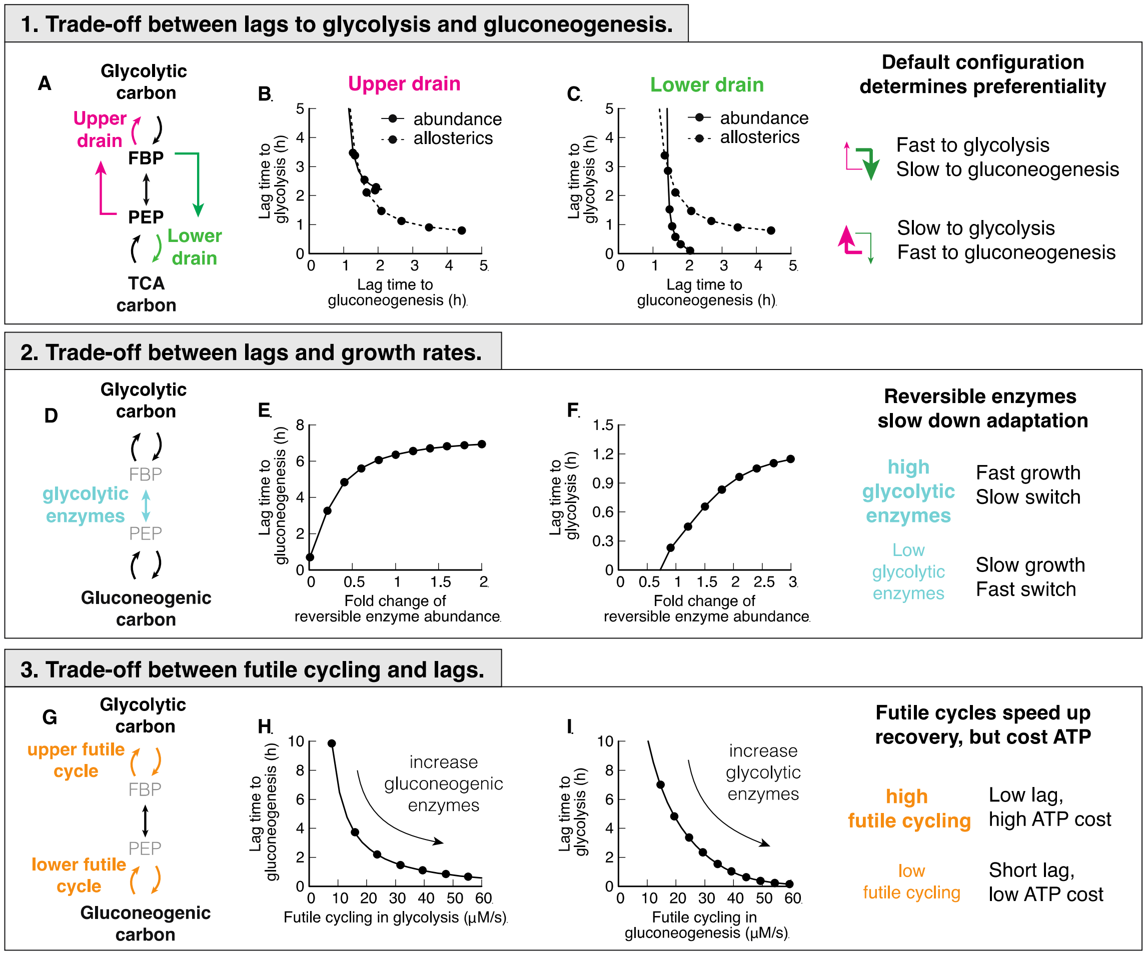

*Figure 5 Trade-offs between glycolysis and gluconeogenesis. (**A**) Two drains in central metabolism deplete central metabolites. (**B-C**) Changing abundance ϕ or allosteric regulation strength α in either lower or upper drain leads to a shift of lag times, decreasing lags in one direction at the cost of the other. Chosing strength of the drains such that either top or bottom is stronger, will lead to a fast recovery in on direction, and a slow in the other. (**D**) Reversible enzymes in the central metabolism (coarse-grained here into 'super-eno'). Abundance of reversible enzymes scale linearly with growth rate [16]. (**E-F**) Decreasing abundance of reversible enzymes decreases lag times. This effect is due to regulatory metabolites being in a far-from-equilibrium state when abundances are low, which allows differential regulation via FBP and PEP. For high abundance, regulation is weak and lag times long. (**G**) There are two futile cycles in central metabolism. (**H-I**) Increasing abundance of enzymes of the opposing direction in pre-shift, e.g. gluconeogenic enzymes in glycolytic growth, increases futile cycling and decreases lag times. Because in futile cycles free energy is dissipated, usually in the form of ATP hydrolysis, futile cycling has an energetic cost.*

Three trade-offs constrain lag times to glycolysis and gluconeogenesis

The out-of equilibrium state is caused by net flux going through metabolism. Therefore, we investigated what causes fluxes not to flow in a uniform direction after shifts to glycolysis and gluconeogenesis. In principle, metabolite flux brought into central metabolism can exit via two drains: upper gluconeogenesis, activated by PEP, and lower glycolysis, activated by FBP (Fig. 5A). If the strength of the lower drain is stronger than the upper drain, then after a switch to glycolysis, FBP builds up, PEP is drained and a net flux is immediately accomplished. In a shift to gluconeogenesis, however, the lower drain leaks the influx coming from the bottom, as seen in Fig. 3F, leading to an in-and-out flux, but no net flux. In this situation, FBP and PEP stay in equilibrium and the recovery stalls. If on the other hand, the upper drain was stronger than the lower drain, then we would expect the behavior to be reversed and gluconeogenic flux would be immediately accomplished, while the glycolytic recovery would stall.

In the simulation, we are able test the hypothesis that the strength of the upper and lower drains determines the preferential directionality of the central metabolism (Fig. 5B&C) by varying enzyme abundances and the strength of allosteric interactions in upper (pink) and lower drains (green) *in silico*, and letting metabolism adapt to gluconeogenesis and glycolysis conditions. Indeed, we found that a decrease of lag time in one direction led to an increase of lag time in the opposite direction.

Varying the outflow from metabolism is not the only determinant of lag times. The set of reversible enzymes, coarse-grained in our model into 'super-eno', plays another key role, because they interconvert the regulatory metabolites FBP and PEP (Fig. 5D). If this conversion is fast, the concentrations of FBP and PEP will be close to their equilibrium relation in Eq. (7), and differential regulation is impossible. As a result, lag times in both directions increase if the abundance of reversible reactions increase (Fig. 5E-F). This is a counter-intuitive result, as one would have naïvely expected more enzymes to speed up reactions. But instead, in metabolism more enzymes will collapse the differential regulation and slow down adaptation rates. Because the cell needs to scale the abundance of reversible glycolytic enzymes with growth rate to catalyze sufficient flux through metabolism, the relation between reversible enzyme abundance and lag time is in fact a fundamental trade-off between growth rate and lag time.

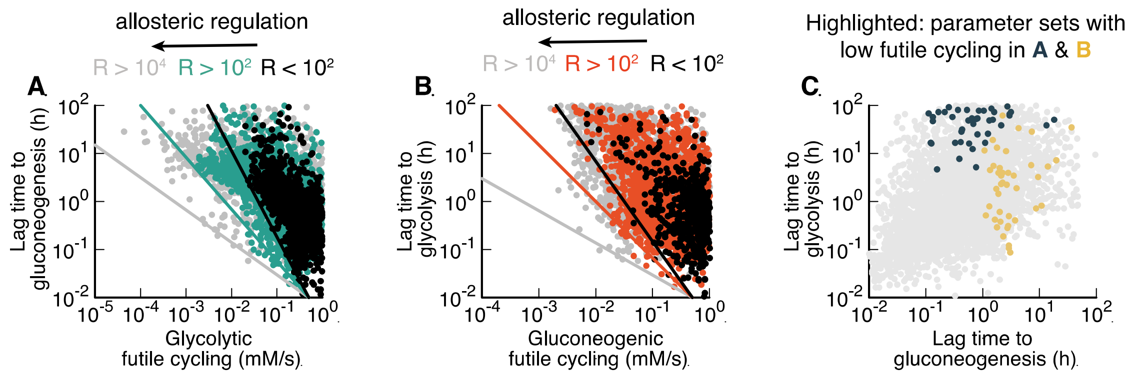

*Figure 6 Large-scale parameter scan reveals Pareto optimality between lag times and futile cycling. (**A-B**) Model calculated for randomized protein abundancies, reaction rates, Michaelis constants, allosteric interactions, transcriptional regulation, see SI. Each point corresponds to a parameter set that allows exponential growth on both glycolytic and gluconeogenic carbons, as well switching between both conditions. Data is colored according to the total regulation R, i.e., sum of fold-changes of enzyme activities between glycolysis and gluconeogenesis, $\left(c_i^{gly}/c_i^{gng}\right)^{\alpha_i}$. For standard E. coli parameters R = 23. R>10⁴ are likely unphysiological. Lines indicate Pareto front. (**C**) Parameter sets from panels A&B with low futile cycling highlighted over the background of all parameter sets (grey).*

Finally, we found that while lag times are constrained by the two above trade-offs, they can be substantially decreased if the cell allows more futile cycling, i.e., the circular conversion of metabolites in the upper and lower irreversible reactions that dissipates ATP (Fig. 5G). Increasing the abundance of gluconeogenic enzymes in glycolytic growth (Fig. 5H) or glycolytic enzymes in gluconeogenic growth (Fig. 5I) substantially decreases lag times at the cost of futile cycling, which dissipates free energy in the form of ATP. This third trade-off thus allows organisms to decrease their switching times by sacrificing energetic efficiency.

Because the three trade-offs of Fig. 5 are based on a single parameter set, the same as in Fig. 1-4, we wondered if different biochemical parameters and regulations could break the trade-offs and allow simultaneous fast growth and fast switching without costly futile cycling. To investigate this possibility, we performed an extensive scan of model parameters, by randomly choosing sets of biochemical parameters and simulating the resulting model. Of those parameter sets, we chose those that allowed steady state growth in both glycolytic and gluconeogenic conditions, and were able to switch between both states. We found that metabolism in the majority of randomly generated models is inefficient and dominated by futile cycling in upper and lower glycolysis; only a minority of models were able to reduce futile cycling in glycolysis and gluconeogenesis.

Remarkably, despite probing variations of all possible model parameters, including Michaelis Menten parameters of enzymes and the strengths of allosteric and transcriptional regulation, lag times could not be reduced at-will by the cell. Instead, a ‘Pareto frontier’ between futile cycling in preshift conditions and lag times emerged (Fig. 6 A&B). Points close to the ‘Pareto frontier’ (solid lines) are Pareto-optimal, meaning that any further decrease of either parameter must come at the expense of the other. Overall, stronger allosteric regulation (black: $R < 10^2$, red/green: $R > 10^2$, grey: $R > 10^4$) shifted the Pareto frontier, but was not able to overcome it. Parameter combinations that led to low futile cycling in either glycolysis or gluconeogenesis showed long lag times in at least one condition (Fig. 6C). Thus, from this analysis, it seems that organisms cannot overcome long lag times without paying a futile cycling cost during steady-state growth.

Pseudomas aeruginosa is at the other end of Pareto spectrum

Taken together, the results of Fig. 5 & 6 suggest that the cell cannot achieve fast growth, low futile cycling and fast adaptation simultaneously in both glycolysis and gluconeogenesis. Instead, each of the three trade-offs will constrain the evolutionary optimization of microbial metabolism, such that any optimal solution is on a the surface of a multidimensional Pareto frontier, where any improvement in one phenotype will come at the expense of another.

Because the preference is solely determined by biochemical parameters that are not strongly constrained, such as strengths of allosteric regulations and enzyme abundances, it could be reversed during evolutionary adaptation if bacteria evolve on gluconeogenic substrates. From the model, we expect that microbes should exist that show precisely the opposite phenotypic pattern of *E. coli*: fast switching to gluconeogenic substrates, where *E. coli* shows long lag phases, and slow switching to glycolytic substrates, where *E. coli* adapts quickly.

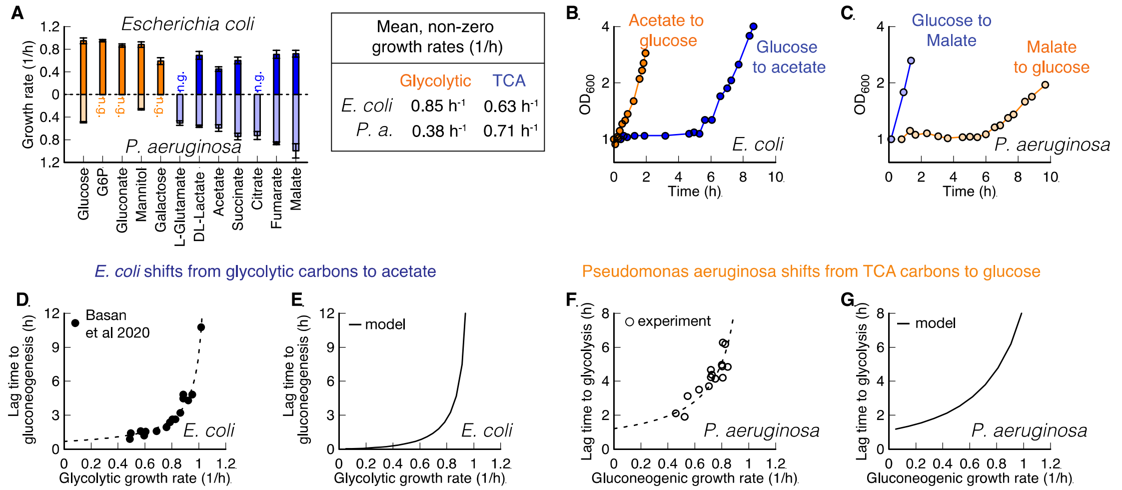

*Figure 7 Comparison of Escherichia coli and Pseudomonas aeruginosa during growth and shifts. (**A**) Growth rates on glycolytic carbons (orange) are faster for E. coli than on gluconeogenic carbons (blue). For Pseudomonas, this dependence is reversed. No growth indicated with "n.g". (**B-C**) Shifts for E. coli and P. aeruginosa between glycolytic and gluconeogenic carbon substrates. The preferential order of P. aeruginosa is reversed in comparison to E. coli (**D**) E. coli shows an increase of lag times to gluconeogenesis with increasing pre-shift growth rate. Lag times diverge around growth rate 1.1/h. (**E**) The model predicts diverging growth rates without further fitting, based on the growth rate dependent expression levels of glycolytic and gluconeogenic enzymes (Fig. 2E-F). (**F**) P. aeruginosa shows a strikingly similar growth rate to lag time dependence as E. coli, when switched to glycolysis, with lag times diverging around 1.0/h. (**G**) The model can recapitulate observed P. aeruginosa lag times if pre-shift glycolytic enzymes are decreased as a function of pre-shift growth rate.*

One possible example of such microbes are *Pseudomonas* species, which have been reported to show diauxie when switching from glycolytic to gluconeogenic substrates (Lynch and Franklin, 1978). Therefore, we tested the model predictions in a strain of the clinically relevant species, *P. aeruginosa*. Indeed, we found that *P. aeruginosa* grew faster on gluconeogenic carbon substrates, than on glycolytic carbon substrates, which is the opposite preference of *E. coli* (Fig. 7A). In addition, *P. aeruginosa* showed the reversed lag time phenotypes compared to *E. coli* (compare Fig. 7C & D), i.e. short lag phase when shifted from glycolysis (glucose) to gluconeogenesis (malate), but a long lag phase in the opposite direction. (Fig. 7C).

In Basan et al (Basan et al., 2020) it was shown that lag times to gluconeogenesis for *E. coli* depend on the pre-shift growth rate (Fig. 7D). Our kinetic model captures the divergence of lag times at fast growth rate, simply by varying the carbon uptake rate in the pre-shift condition (Fig. 7E), because the increase of lag time is caused by the linear decrease of gluconeogenic enzyme abundance (Fig. 2B), and increase of glycolytic enzyme abundance (Fig. 2C) with faster growth rate, which are already implemented via the FBP-cra regulation in the model (see Box 1). While glycolytic enzymes are required to ensure sufficient glycolytic flux, the reduction of gluconeogenic enzymes reduces the backward flux that causes futile cycling.

If *Pseudomonas aeruginosa* is subject to the same trade-offs as *E. coli*, then we expect it to have evolved a similar regulation. Fast growing *P. aeruginosa* should have a low abundance of glycolytic enzymes, to reduce futile cycling and allow efficient growth. Slow growing *P. aeruginosa* should have higher glycolytic abundance and show shorter lag times. To test this hypothesis, we grew *P. aeruginosa* on a variety of TCA carbons (same as in Fig. 6A) and shifted to glucose. Indeed, we observe an increase of lag time for faster growth that is remarkably similar to what we previously found for *E. coli* (Fig. 6F). The increase of lag times can be captured by the model, by varying the expression of glycolytic enzymes, i.e. varying futile cycling, in the pre-shift condition (Fig. 6E). This demonstrates that *P. aeruginosa* is constrained by the same trade-offs between growth and lag that are present for *E. coli*. However, in contrast to *E. coli*, *P. aeruginosa* appears to have evolutionarily chosen a different objective, and evolved fast and efficient gluconeogenic growth, as well as fast switching to gluconeogenesis. *P. aeruginosa* is thus located at the opposite spectrum of the Pareto frontier compared to *E. coli*.

Discussion

In this work, we presented a self-consistent, coarse-grained kinetic model of central carbon metabolism, combining key allosteric and transcriptional regulation, as well as biomass production, enzyme synthesis, and growth. This model elucidates the remarkable capacity of central carbon metabolism to self-organize in response to substrate availability and flux requirements. The simulation successfully recapitulates enzyme and metabolite levels for different glycolytic growth rates, as well as growth rate and metabolite dynamics of growth shifts, as measured previously in *E. coli*. But the model also reveals key limitations to this flux-sensing based self-organization that can only be partially overcome at a cost determined by three fundamental tradeoffs between growth rate, futile cycing and lag times for shifts to the non-preferred direction. This suggests that central carbon metabolism inherently has a preferred flux direction that should evolve in different organisms, depending on the ecological environment and preferential substrate utilization. We validated this key model prediction in a different bacterial species, *P. aeruginosa* and showed that in *P. aeruginosa*, reversal of substrate preference as compared to *E. coli*, coincides with a complete reversal of the phenomenology of lag phases and tradeoffs during shifts between different substrates.

Our model indicates microbes could in principle reduce lag times by tolerating high levels of futile cycling. We estimate that ATP dissipation from futile cycling can be on the same order of magnitude as the energy budget of the cell during steady-state growth, but energy production pathways only constitute a relatively small fraction (around 20%) of the total cellular proteome (Basan et al., 2015a). Thus, in theory, the cell might be able to compensate for higher levels of futile cycling with increasing resources devoted to energy production. However, experimentally it appears that *E. coli* chooses to keep futile cycling in check, even at the cost of substantially reduced growth rates, as evidenced by the repression of glycolytic enzymes by the transcription factor Cra resulting in slower growth (Basan et al., 2020). We hypothesize that futile cycling must be considered not just during steady-state growth, but during growth shifts and during starvation, where the cellular energy budget is much more limited. In fact, it has been recently shown that the energy budget of the cell is around 100-fold smaller during carbon starvation and that energy dissipation can increase death rates several-fold (Schink et al., 2019). Therefore, even levels of futile cycling that are modest during steady-state growth should severely affect survival of cells in these conditions.

Our findings indicate that lag times and a tradeoff between futile cycling and short lag times are inherent properties of central carbon metabolism, at least given the existing allosteric and transcriptional regulation. Why different regulation that can overcome this limitation has not evolved, at least in the microbes that we tested, is a difficult question. In principle, one could imagine that the cell could directly detect the presence of gluconeogenic substrates and the absence of glycolytic substrates, which could trigger the active degradation of glycolytic enzymes and would allow the cell to overcome lag phases more quickly. However, since there are dozens of glycolytic and gluconeogenic substrates, this would result in a much higher degree of complexity of the regulation. It may be difficult for a regulatory network to integrate so many signals, many of which would be conflicting with each other in any one condition. Typically, the regulatory architecture found in *E. coli* is of a much simpler in nature (Kochanowski et al., 2013a). The wrong decision to degrade key metabolic enzymes would have adverse consequences, for example when glycolytic flux is only briefly interrupted, degrading these enzymes would impair growth.

Another reason, why no such regulation has evolved could be related the to the striking observation that the regulation of upper and lower glycolysis/gluconeogenesis and directionality of flux are performed by the metabolite concentrations of FBP and PEP, which are cut off from the rest of metabolism by irreversible reactions. We argue that the logic for this regulatory architecture is product inhibition, which ensures that this essential part of central carbon metabolism is adequately supplied with metabolites, but also ensures that uncontrolled accumulation of metabolites does not occur. In fact, because the reactions of upper and lower glycolysis are effectively irreversible, even a slight misbalance in flux between these enzymes and biomass demand would result in uncontrolled accumulation of metabolites and in the absence of a cellular overflow mechanism, these metabolites would quickly reach toxic levels, e.g., via their osmotic activities. As demonstrated by the simulation, the existing regulation of glycolysis/gluconeogenesis successfully solves this potentially serious problem.

Our model shows that the known regulatory architecture of glycolysis/gluconeogenesis accomplishes efficient regulation of fluxes and metabolite pools in response to diverse external conditions, while avoiding toxic accumulation of internal metabolites and integrating multiple conflicting signals with only two regulatory nodes. The glycolysis/gluconeogenesis system is a remarkable example of self-organization of regulatory networks in biology. It provides an elegant solution to the complex, obligatory problem, posed by the biochemistry of central carbon metabolism. All organisms that need to switch between glycolytic and gluconeogenic flux modes face this problem and we argue that this explains the striking degree of conservation of the phenomenology of shifts between glycolytic and gluconeogenic conditions that we found in different microbial species, ranging from *E. coli*, *Bacillus subtilis*, and even wild-type strains of the lower eukaryote *Saccharomyces cerevisiae* to the reversed phenotypes in *P. aeruginosa*. Conversely, we argue that the quantitative phenotypes exhibited by microbes in such idealized growth shift experiments in the lab, can reveal much about their natural environments, ecology and evolutionary origin.

Acknowledgments

We thank Terence Hwa for many fruitful discussions throughout this project. This project was financed by MIRA grant (5R35GM137895) via MB and HFSP Long-term fellowship (LT000597/2018) via SJS.

Author contributions

All authors contributed to the design of the project and writing the manuscript. SJS, DC and MB performed modelling. AM and MB performed experiments.

Methods

Bacterial cultures

Strains used in this paper are wild-type *Escherichia coli* K-12 NCM3722 (Soupene et al., 2003) and *Pseudomonas aeruginosa* PAO1 (Stover et al., 2000). The culture medium used in this study is $N^{-}C^{-}$ minimal medium (Csonka et al., 1994), containing K_2SO_4 (1 g), $K_2HPO_4{\cdot}3H_2O$ (17.7 g), KH_2PO_4 (4.7 g), $MgSO_4{\cdot}7H_2O$ (0.1 g) and NaCl (2.5 g) per liter. The medium was supplemented with 20mM NH_4Cl, as nitrogen source, and either of the following carbon sources: 20mM Glucose-6-phosphate, 20mM gluconate, 0.2% glucose, 20mM succinate, 20mM acetate, 20mM citrate, 20mM malate or 20mM fumerate.

Growth was then carried out at 37° C in a water bath shaker at 200 rpm, in silicate glass tubes (Fisher Scientific) closed with plastic caps (Kim Kap). Cultures spent at least 10 doublings in exponential growth in pre-shift medium. For growth shifts, cultured were transferred to a filter paper and washed twice with pre-warmed post-shift medium. Cells were resuspended from the filter paper in post-shift medium, and unsequently diluted to an OD of about 0.05.

Theoretical modelling

The integrated minmal model of metabolism and growth was implemented in MATLAB using the SimBiology toolbox, and is described in detail in the Supporting Information.

References

Andreozzi, S., Miskovic, L., and Hatzimanikatis, V. (2016). iSCHRUNK – In Silico Approach to Characterization and Reduction of Uncertainty in the Kinetic Models of Genome-scale Metabolic Networks. Metabolic Engineering *33*, 158–168.

Basan, M., Hui, S., Okano, H., Zhang, Z., Shen, Y., Williamson, J.R., and Hwa, T. (2015a). Overflow metabolism in Escherichia coli results from efficient proteome allocation. Nature *528*.

Basan, M., Zhu, M., Dai, X., Warren, M., Sévin, D., Wang, Y.-P., and Hwa, T. (2015b). Inflating bacterial cells by increased protein synthesis. Mol Syst Biol *11*.

Basan, M., Hui, S., and Williamson, J.R. (2017). ArcA overexpression induces fermentation and results in enhanced growth rates of E. coli. Scientific Reports *7*.

Basan, M., Honda, T., Christodoulou, D., Hörl, M., Chang, Y.-F., Leoncini, E., Mukherjee, A., Okano, H., Taylor, B.R., Silverman, J.M., et al. (2020). A universal trade-off between growth and lag in fluctuating environments. Nature.

Bennett, B.D., Kimball, E.H., Gao, M., Osterhout, R., Van Dien, S.J., and Rabinowitz, J.D. (2009). Absolute metabolite concentrations and implied enzyme active site occupancy in Escherichia coli. Nature Chemical Biology *5*, 593–599.

Berger, S.A., and Evans, P.R. (1991). Steady-state fluorescence of Escherichia coli phosphofructokinase reveals a regulatory role for ATP. Biochemistry *30*, 8477–8480.

Berman, K.M., and Cohn, M. (1970). Phosphoenolpyruvate Synthetase of Escherichia coli. Journal of Biological Chemistry *245*, 5309–5318.

Bordbar, A., Monk, J.M., King, Z.A., and Palsson, B.O. (2014). Constraint-based models predict metabolic and associated cellular functions. Nature Reviews Genetics *15*, 107–120.

Buescher, J.M., Liebermeister, W., Jules, M., Uhr, M., Muntel, J., Botella, E., Hessling, B., Kleijn, R.J., Chat, L.L., Lecointe, F., et al. (2012). Global Network Reorganization During Dynamic Adaptations of Bacillus subtilis Metabolism. Science *335*, 1099–1103.

Chakrabarti, A., Miskovic, L., Soh, K.C., and Hatzimanikatis, V. (2013). Towards kinetic modeling of genome-scale metabolic networks without sacrificing stoichiometric, thermodynamic and physiological constraints. Biotechnology Journal *8*, 1043–1057.

Chassagnole, C., Noisommit-Rizzi, N., Schmid, J.W., Mauch, K., and Reuss, M. (2002). Dynamic modeling of the central carbon metabolism of Escherichia coli. Biotechnology and Bioengineering *79*, 53–73.

Chubukov, V., Gerosa, L., Kochanowski, K., and Sauer, U. (2014). Coordination of microbial metabolism. Nature Reviews Microbiology *12*, 327–340.

Cortay, J.C., Nègre, D., Scarabel, M., Ramseier, T.M., Vartak, N.B., Reizer, J., Saier, M.H., and Cozzone, A.J. (1994). In vitro asymmetric binding of the pleiotropic regulatory protein, FruR, to the ace operator controlling glyoxylate shunt enzyme synthesis. The Journal of Biological Chemistry *269*, 14885–14891.

Donahue, J.L., Bownas, J.L., Niehaus, W.G., and Larson, T.J. (2000). Purification and Characterization ofglpX-Encoded Fructose 1,6-Bisphosphatase, a New Enzyme of the Glycerol 3-Phosphate Regulon of Escherichia coli. Journal of Bacteriology *182*, 5624–5627.

Fenton, A.W., and Reinhart, G.D. (2009). Disentangling the web of allosteric communication in a homotetramer: heterotropic inhibition in phosphofructokinase from Escherichia coli. Biochemistry *48*, 12323–12328.

Folly, B.B., Ortega, A.D., Hubmann, G., Bonsing-Vedelaar, S., Wijma, H.J., Meulen, P. van der, Milias-Argeitis, A., and Heinemann, M. (2018). Assessment of the interaction between the flux-signaling metabolite fructose-1,6-bisphosphate and the bacterial transcription factors CggR and Cra. Molecular Microbiology *109*, 278–290.

Gerosa, L., Haverkorn van Rijsewijk, B.R.B., Christodoulou, D., Kochanowski, K., Schmidt, T.S.B., Noor, E., and Sauer, U. (2015a). Pseudo-transition Analysis Identifies the Key Regulators of Dynamic Metabolic Adaptations from Steady-State Data. Cell Systems *1*, 270–282.

Gerosa, L., Haverkorn van Rijsewijk, B.R.B., Christodoulou, D., Kochanowski, K., Schmidt, T.S.B., Noor, E., and Sauer, U. (2015b). Pseudo-transition Analysis Identifies the Key Regulators of Dynamic Metabolic Adaptations from Steady-State Data. Cell Systems *1*, 270–282.

Hines, J.K., Fromm, H.J., and Honzatko, R.B. (2006). Novel Allosteric Activation Site in Escherichia coli Fructose-1,6-bisphosphatase *.

Hui, S., Silverman, J.M., Chen, S.S., Erickson, D.W., Basan, M., Hwa, T., and Williamson, J.R. (2015). Quantitative proteomic analysis reveals a simple strategy of global resource allocation in bacteria. Molecular Systems Biology.

Johnson, J.L., and Reinhart, G.D. (1997). Failure of a two-state model to describe the influence of phospho(enol)pyruvate on phosphofructokinase from Escherichia coli. Biochemistry *36*, 12814–12822.

Kelley-Loughnane, N., Biolsi, S.A., Gibson, K.M., Lu, G., Hehir, M.J., Phelan, P., and Kantrowitz, E.R. (2002). Purification, kinetic studies, and homology model of Escherichia coli fructose-1,6-bisphosphatase. Biochimica et Biophysica Acta *1594*, 6–16.

Kochanowski, K., Volkmer, B., Gerosa, L., Haverkorn van Rijsewijk, B.R., Schmidt, A., and Heinemann, M. (2013a). Functioning of a metabolic flux sensor in Escherichia coli. Proceedings of the National Academy of Sciences *110*, 1130–1135.

Kochanowski, K., Volkmer, B., Gerosa, L., Haverkorn van Rijsewijk, B.R., Schmidt, A., and Heinemann, M. (2013b). Functioning of a metabolic flux sensor in Escherichia coli. Proceedings of the National Academy of Sciences of the United States of America *110*, 1130–1135.

Kotte, O., Volkmer, B., Radzikowski, J.L., and Heinemann, M. (2014). Phenotypic bistability in Escherichia coli's central carbon metabolism. Molecular Systems Biology *10*, 736.

Link, H., Anselment, B., and Weuster-Botz, D. (2008). Leakage of adenylates during cold methanol/glycerol quenching of Escherichia coli. Metabolomics *4*, 240–247.

Link, H., Kochanowski, K., and Sauer, U. (2013). Systematic identification of allosteric protein-metabolite interactions that control enzyme activity in vivo. Nature Biotechnology *31*, 357–361.

Lynch, W.H., and Franklin, M. (1978). Effect of Temperature on Diauxic Growth with Glucose and Organic Acids in Pseudomonas fluorescens.

Noor, E., Eden, E., Milo, R., and Alon, U. (2010). Central Carbon Metabolism as a Minimal Biochemical Walk between Precursors for Biomass and Energy. Molecular Cell *39*, 809–820.

Noor, E., Bar-Even, A., Flamholz, A., Reznik, E., Liebermeister, W., and Milo, R. (2014). Pathway Thermodynamics Highlights Kinetic Obstacles in Central Metabolism. PLOS Computational Biology *10*, e1003483.

Otterstedt, K., Larsson, C., Bill, R.M., Ståhlberg, A., Boles, E., Hohmann, S., and Gustafsson, L. (2004). Switching the mode of metabolism in the yeast Saccharomyces cerevisiae. EMBO Reports *5*, 532–537.

Pham, A.S., and Reinhart, G.D. (2001). Pre-steady state quantification of the allosteric influence of Escherichia coli phosphofructokinase. J Biol Chem *276*, 34388–34395.

Ramseier, T.M., Bledig, S., Michotey, V., Feghali, R., and Saier, M.H. (1995). The global regulatory protein FruR modulates the direction of carbon flow in Escherichia coli. Molecular Microbiology *16*, 1157–1169.

Saa, P., and Nielsen, L.K. (2015). A General Framework for Thermodynamically Consistent Parameterization and Efficient Sampling of Enzymatic Reactions. PLOS Computational Biology *11*, e1004195.

Schink, S.J., Biselli, E., Ammar, C., and Gerland, U. (2019). Death Rate of E. coli during Starvation Is Set by Maintenance Cost and Biomass Recycling. Cell Systems *9*, 64-73.e3.

Soupene, E., van Heeswijk, W.C., Plumbridge, J., Stewart, V., Bertenthal, D., Lee, H., Prasad, G., Paliy, O., Charernnoppakul, P., and Kustu, S. (2003). Physiological Studies of

Escherichia coli Strain MG1655: Growth Defects and Apparent Cross-Regulation of Gene Expression. J Bacteriol *185*, 5611–5626.

Stincone, A., Prigione, A., Cramer, T., Wamelink, M.M.C., Campbell, K., Cheung, E., Olin-Sandoval, V., Grüning, N.-M., Krüger, A., Alam, M.T., et al. (2015). The return of metabolism: biochemistry and physiology of the pentose phosphate pathway. Biological Reviews *90*, 927–963.

Stover, C.K., Pham, X.Q., Erwin, A.L., Mizoguchi, S.D., Warrener, P., Hickey, M.J., Brinkman, F.S.L., Hufnagle, W.O., Kowalik, D.J., Lagrou, M., et al. (2000). Complete genome sequence of Pseudomonas aeruginosa PAO1, an opportunistic pathogen. Nature *406*, 959–964.

Valentini, G., Chiarelli, L., Fortini, R., Speranza, M.L., Galizzi, A., and Mattevi, A. (2000). The allosteric regulation of pyruvate kinase: A site-directed mutagenesis study. Journal of Biological Chemistry *275*, 18145–18152.

Vasilakou, E., Machado, D., Theorell, A., Rocha, I., Nöh, K., Oldiges, M., and Wahl, S.A. (2016). Current state and challenges for dynamic metabolic modeling. Current Opinion in Microbiology *33*, 97–104.

Yang, L., Ebrahim, A., Lloyd, C.J., Saunders, M.A., and Palsson, B.O. (2019). DynamicME: dynamic simulation and refinement of integrated models of metabolism and protein expression. BMC Systems Biology *13*, 2.

Zampar, G.G., Kümmel, A., Ewald, J., Jol, S., Niebel, B., Picotti, P., Aebersold, R., Sauer, U., Zamboni, N., and Heinemann, M. (2013). Temporal system-level organization of the switch from glycolytic to gluconeogenic operation in yeast. Molecular Systems Biology *9*, 651.

Zheng, R.L., and Kemp, R.G. (1995). Phosphofructo-1-kinase: Role of Charge Neutralization in the Active Site. Biochemical and Biophysical Research Communications *214*, 765–770.